

Bachelor's Thesis

Studien von Top-Quark-Paaren in $\sqrt{s}=8$ TeV Daten mit dem ATLAS-Experiment

Studies of top-quark pairs in $\sqrt{s}=8$ TeV data collected with the ATLAS experiment

prepared by

Jens Oltmanns

from Norden

at the II. Physikalisches Institut

Thesis number: II.Physik-UniGö-BSc-2014/06
Thesis period: 14th April 2014 until 18th July 2014
First referee: Prof. Dr. Arnulf Quadt
Second referee: Prof. Dr. Ariane Frey

Abstract

The signature of a decay process is not unique. Instead, there are other processes with the same signature. These processes are called background processes. Control plots are made to estimate the fraction of the background processes in the given data. PlotFactory is a programme used to produce such plots. This thesis is about the modifications implemented in the PlotFactory.

The modifications are renewing the HTML page produced by thy PlotFactory to make the page clearer and to make the navigation between different sites easier. Pseudo top distributions are added to the analysis. Those are used for a measurement of the top quark decay width. Also plots with logarithmic axis are included and goodness-of-fit tests are applied.

Zusammenfassung

Die Signatur eines Zerfallsprozesses ist nicht einzigartig, sondern es gibt andere Prozesse, deren Signatur dieselbe ist. Diese Prozesse werden Untergrundprozesse genannt. Um eine Abschätzung des Anteils der Untergrundprozesse an den gemessenen Daten zu haben, werden Controlplots gemacht. Ein Programm, das Controlplots erstellt, ist PlotFactory. In dieser Bachelorarbeit geht es um die Modifikationen, die während des Bachelorprojekts an der PlotFactory vorgenommen wurden.

Die Modifikationen waren die vom Programm ausgegebene HTML Seite zu überarbeiten, um diese übersichtlicher zu machen und die Navigation zwischen verschiedenen Seiten zu erleichtern. Ebenfalls wurde eine Analyse von Pseudo Top-Quarks hinzugefügt, welche für die Messung der Zerfallsbreite des Top-Quarks benötigt werden. Des weiteren wurden die Controlplots durch weitere Plots mit logarithmischer Achse erweitert und Goodness-of-Fit Tests in den Plots ergänzt, um die Übereinstimmung von aufgenommen und generierten Daten zu bewerten.

Contents

| | | |
|----------|--|-----------|
| 1 | Introduction | 1 |
| 2 | Theoretical Fundamentals | 3 |
| 2.1 | Standard Model of Particle Physics | 3 |
| 2.1.1 | Leptons and Quarks | 3 |
| 2.1.2 | Bosons and Interactions | 4 |
| 2.1.3 | Higgs Mechanism | 6 |
| 2.2 | Top Quark | 6 |
| 2.2.1 | Top Quark Properties | 6 |
| 2.2.2 | Top Quark Production | 7 |
| 2.2.3 | Top Quark Decay | 9 |
| 3 | Experimental Setup | 13 |
| 3.1 | Large Hadron Collider | 13 |
| 3.2 | The ATLAS Detector | 14 |
| 3.2.1 | Inner Detector | 14 |
| 3.2.2 | Calorimeter System | 15 |
| 3.2.3 | Muon Spectrometer | 15 |
| 3.2.4 | Trigger System | 16 |
| 4 | Fundamentals of the Analysis | 17 |
| 4.1 | Background Processes | 17 |
| 4.2 | Simulated Events and Data Samples | 18 |
| 4.3 | b -Tagging | 19 |
| 4.4 | D3PD | 19 |
| 4.5 | Kinematic Quantities | 20 |
| 5 | TopRootCore | 23 |
| 5.1 | The Software Package TopRootCore | 23 |
| 5.2 | PlotFactory | 23 |

Contents

| | | |
|----------|---------------------------------------|-----------|
| 6 | Results | 25 |
| 6.1 | HTML Page | 27 |
| 6.2 | Pseudo Top Distributions | 28 |
| 6.3 | Goodness-of-Fit Test | 30 |
| 6.3.1 | χ^2 Test | 31 |
| 6.3.2 | Kolmogorow-Smirnow Test | 32 |
| 6.4 | Logarithmic Scale Plots | 32 |
| 6.5 | Modifications of the Layout | 33 |
| 7 | Conclusion | 35 |
| A | Additional Plots | 37 |

1 Introduction

Particle physicists search for the fundamental components of matter and how they interact with each other. Within the last century, many elementary particles could be found and described by the Standard Model of Particle Physics, which is the theoretical foundation of particle physics. This theory was tested in many different experiments, most of them based on particle accelerators. In those machines, particles are accelerated to high energies and afterwards collided. Therefore particle physics is often also called *High Energy Physics*. To observe smaller structures and find heavier particles, colliders with larger energies are needed.

At present, the collider with the highest energy is the Large Hadron Collider (LHC) at CERN in Geneva, which is designed for a beam energy of 7 TeV and a centre-of-mass energy of 14 TeV. At this energies, it is possible to search for particles which are not included in the Standard Model, like supersymmetric particles.

One particle in the Standard Model is the top quark, which has some unique quantities making it very interesting for particle physics. The top quark is the heaviest particle in the Standard Model. Its mass is of the order of heavy atoms like gold and its lifetime is very short, of the order of 10^{-25} s. The high mass makes the top quark a good candidate to find physics which is not explained in the Standard Model.

A lot of top quarks are produced at the Large Hadron Collider, most of them in $t\bar{t}$ events, with the top (t) and the antitop (\bar{t}), and less frequently as single tops. The top quark decays in different decay channels, each with a specific signature. This signature is not unique, but there are different other processes having the same signature, which are called background processes. To estimate the influence of these processes on the results, control plots are made. There are different programmes to create these plots, one of them is PlotFactory, a package implemented in TopRootCore. The main part of the bachelor project was to modify this programme in order to have a better overview of the results and to add new analysis steps.

1 Introduction

The following Chapter 2 will give a short introduction to the Standard Model and also an overview of top quark physics. In Chapter 3, the experimental setup will be discussed. The fundamentals needed for the analysis will be explained in Chapter 4. A short introduction into TopRootCore and the PlotFactory will be given in Chapter 5. In Chapter 6, the results of the bachelor project are presented, followed by a conclusion in Chapter 7. In this thesis natural units with $c = \hbar = 1$ are used.

2 Theoretical Fundamentals

2.1 Standard Model of Particle Physics

The Standard Model of Particle Physics, often shortened as SM, is a theory to explain particles and their interaction on the smallest level. It emerged from 1960 to 1970. The interactions explained by the SM are the strong interaction, the weak interaction and the electromagnetic interaction. Not included in the SM is the interaction caused by gravity, which is negligible at the today observable energy scales.

The described particles are arranged into fermions and bosons, while fermions are sorted into leptons and quarks. The bosons are mediating the forces between the particles and are called mediators.

Nowadays effects are known which can not be explained by the SM, for example finite masses of neutrinos or the existence of dark matter in the universe.

2.1.1 Leptons and Quarks

In this section the aforementioned fermions will be discussed in more detail. As introduced above, the fermions are sorted in two substructures, the quarks and the leptons.

The six different leptons and quarks are grouped into three generations, which differ in the masses of the particles. The first generation is the lightest generation and the third generation the heaviest. All fermions are spin-1/2-particles.

The leptons are sorted by isospin I_3 , electron number L_e , muon number L_μ and tau number L_τ in the following way:

$$\begin{pmatrix} \nu_e \\ e \end{pmatrix}, \quad \begin{pmatrix} \nu_\mu \\ \mu \end{pmatrix}, \quad \begin{pmatrix} \nu_\tau \\ \tau \end{pmatrix}. \quad (2.1)$$

When including the handedness, the left-handed leptons and lepton-neutrinos form doublets, while the right-handed leptons form singlets and right-handed neutrinos do not exist. The lepton e is called electron, the μ muon and the τ tau lepton. These three leptons have a charge of $-e$, where e denotes the elementary charge. The ν_e , ν_μ and ν_τ

2 Theoretical Fundamentals

are the corresponding neutrinos to the charged leptons. These particles are electrically neutral, as their name indicates.

The quarks are organised similar to the leptons by their isospin I_3 , upness U , downness D , strangeness S , charmness C , bottomness B and topness T in the following way:

$$\begin{pmatrix} u \\ d \end{pmatrix}, \quad \begin{pmatrix} c \\ s \end{pmatrix}, \quad \begin{pmatrix} t \\ b \end{pmatrix}. \quad (2.2)$$

The *Up-type* quarks u , c , t are called Up, Charm, and Top quark. These quarks carry an electric charge of $+2/3e$. The *Down-type* quarks d , s , b are called Down, Strange, Bottom quark and carry an electric charge of $-1/3e$. Unlike the leptons, quarks carry in addition to the electrical charge another charge, called colour charge. There are three different possibilities for the colour charge *red*, *blue* and *green*.

Other quantities next to charge and mass of fermions are the third component of the weak isospin I_3 and the weak hypercharge Y_W , which is given by $Y_W = 2(Q - I_3)$. The particles are arranged that way that the particles with $I_3 = 1/2$ are at the top of the doublet and the particles with $I_3 = -1/2$ are the bottom.

For every fermion there is an antiparticle. The antiparticle has the same mass as the corresponding particle but a different charge and the opposite quantum numbers, like the isospin. Neutrinos and antineutrinos, which both do not have charge, differ in their isospin and their handedness. Neutrinos are always left-handed, while antineutrinos are always right-handed. Antiquarks also carry an anticolour.

Quarks and antiquarks can not be observed as free particles. They always combine to form bound states or they decay. There are two possibilities for quarks and antiquarks to combine. The first is the combination into mesons, which consist of one quark and one antiquark. The other possibility are baryons or antibaryons which consist of three quarks or antiquarks. The process of building bound states is called hadronisation. There is one quark that exists as an almost free particle, the top quark, which decays before it is able to hadronise into a bound state. More about the top quark will be explained in later sections. The mass and charges of all fermions are listed in Table 2.1.

2.1.2 Bosons and Interactions

The bosons are the mediators of the interactions while each interaction has its own type of mediator. The mediator of the electromagnetic interaction is the photon, which is a spin-1-particle without a mass and without electric charge or colour charge. Photons couple to electric charge, so just charged particles take part in the electromagnetic in-

| Lepton | Mass [MeV] | Charge [e] | Quark | Mass [MeV] | Charge [e] |
|------------|----------------------|------------|-------|--------------------------|------------|
| e | 0.510998928 ± 11 | -1 | u | $2.3_{-0.5}^{+0.7}$ | $2/3$ |
| μ | 105.6583715 ± 35 | -1 | d | $4.8_{-0.3}^{+0.7}$ | $-1/3$ |
| τ | 1776.82 ± 0.16 | -1 | c | 1275 ± 25 | $2/3$ |
| ν_e | $> 2 \cdot 10^{-6}$ | 0 | s | 95 ± 5 | $-1/3$ |
| ν_μ | $> 2 \cdot 10^{-6}$ | 0 | t | $173500 \pm 600 \pm 800$ | $2/3$ |
| ν_τ | $> 2 \cdot 10^{-6}$ | 0 | b | 4180 ± 30 | $-1/3$ |

Table 2.1: Masses and charges of the different fermions [1].

teraction. Since photons are electrically neutral, $\gamma - \gamma$ -couplings are not possible. The electromagnetic interaction is described by quantum electrodynamics.

The mediators of the strong interaction are eight gluons which have neither mass nor charge, but carry colour charge and anticolour charge in which they differ. Gluons couple to colour, so only quarks and hadrons take part in the strong interaction. The fact that gluons carry a colour and anticolour themselves makes $g - g$ -couplings possible. The quantum field theory describing the strong interaction is quantum chromodynamics.

The weak interaction can be categorised into charged weak interaction and the neutral weak interaction. The mediators of the charged weak interaction are the W^+ and W^- bosons. They carry a charge of $\pm 1e$ and also have a finite mass of about 80.385 ± 0.15 GeV [1], but do not carry colour charge.

The mediator of the neutral weak interaction is the Z^0 boson. It is not carrying a charge or colour but has, like the W^\pm bosons, a non-zero mass of about 91.1876 ± 0.0021 GeV [1]. This weak interaction is described by quantum flavourdynamics.

In contrast to the other interactions, the charged weak interaction is not flavour conserving, so the charged weak interaction can mix between the generations of the quarks. This mixing is possible because the eigenstates of the weak interaction are not the same as the mass eigenstates. The connections between the weak eigenstates $|d'\rangle, |s'\rangle, |b'\rangle$ and the mass eigenstates $|d\rangle, |s\rangle, |b\rangle$ are given by the CKM matrix in the following way [2]:

$$\begin{pmatrix} |d'\rangle \\ |s'\rangle \\ |b'\rangle \end{pmatrix} = \begin{pmatrix} V_{ud} & V_{us} & V_{ub} \\ V_{cd} & V_{cs} & V_{cb} \\ V_{td} & V_{ts} & V_{tb} \end{pmatrix} \begin{pmatrix} |d\rangle \\ |s\rangle \\ |b\rangle \end{pmatrix}. \quad (2.3)$$

This matrix was established by Kobayashi and Maskawa and is an expansion of the Cabibbo matrix, which is the quark mixing matrix for two generations [3]. The matrix consist of 18 parameters, while 14 are fixed by unitary conditions and choice of phase, what leads to four free parameters, three real angles and one complex phase. This phase is responsible for CP (charge parity) violation.

The electromagnetic and the weak interactions are unified in the electroweak interaction proposed by Glashow, Salam and Weinberg [4–6].

2.1.3 Higgs Mechanism

The effort to formulate the interactions in local gauge theories failed because of the non-zero mass of the mediators in the weak interaction. One solution to this problem is the Higgs-mechanism postulated by Peter Higgs and others in 1964 [7–9]. This theory contains in addition to the three masses of the W^\pm and Z^0 another degree of freedom. This is the mass of another particle, the Higgs-boson, which is a spin-0-particle. The search of this particle took physicists a lot of time, but it was discovered 2012 at the ATLAS and CMS colliders at the Large Hadron Collider at CERN [10, 11]. The discovery was followed by a Nobel prize for Peter Higgs and François Englert in 2012.

2.2 Top Quark

The top quark is a particle in the SM and was discovered in 1995 at the $p\bar{p}$ collider TEVATRON by the experiments CDF and DØ [12, 13]. The production mechanism was $t\bar{t}$ production. Another possible channel is the single top production, which was observed 2009 at the CDF and DØ experiments [14, 15].

2.2.1 Top Quark Properties

The top quark is the weak isospin partner of the bottom quark. This means that its spin is assumed to be $1/2$ and its electrical charge is assumed to be $+2/3e$, but these quantities have not been measured yet. For the charge of the top quark the value of $-4/3e$ has been excluded by several experiments, one of them the ATLAS experiment [16].

What makes the top quark unique and interesting is its heavy mass and its short lifetime. The mass of the top quark is measured by experiments at TEVATRON and LHC. The combined measurement of the four experiments ATLAS, CDF, CMS and DØ had the results in an estimated top quark mass of [17]:

$$173 \pm 0.27(\text{stat}) \pm 0.73(\text{syst}) \text{ GeV}. \quad (2.4)$$

This mass, which is comparable with the mass of atoms like gold, is larger than the mass of the W^\pm boson, what gives the possibility for the top quark to decay into a real W^\pm boson. Other fermions can not decay into a real W^\pm boson because their masses are much

lower than the one of the W^\pm .

The most likely decay of the top quark is the decay $t \rightarrow Wq$, while q can be an arbitrary down-type quark, so d, s or b . This is a weak process and the probability which down-type quark is depending on the matrix element in the CKM matrix $|V_{tq}|^2$. Since the matrix element $V_{tb} \approx 1$ [1], the top quark almost always decays in the way $t \rightarrow Wb$ and the lifetime of the top quark is extremely short, just [18]

$$\tau_t \approx 5 \cdot 10^{-25} \text{ s.} \quad (2.5)$$

This is even shorter than the time quarks need to build bound states. This property makes the top quark the only quark being observed in “bare” form. Because the lifetime is hard to measure, it is more likely to measure the decay width of the top quark and then calculate the lifetime via

$$\tau = \frac{\hbar}{\Gamma}. \quad (2.6)$$

2.2.2 Top Quark Production

Top quarks are produced either in $t\bar{t}$ pairs or as single tops, while the pair-production has a larger cross section. The different production mechanisms with the different decay channels will be shown in the next paragraphs.

$t\bar{t}$ Production The top-antitop pair production is the dominant production process in hadron colliders like TEVATRON or LHC. The production takes place by either $q\bar{q}$ annihilation via $q\bar{q} \rightarrow t\bar{t}$ or gg fusion via $gg \rightarrow t\bar{t}$. In hadron colliders, the partons inside the hadron are the particles taking part in the interaction, not the hadron itself. These processes are mediated by the strong interaction, so by exchange of a gluon. The leading order Feynman diagrams are shown in Figure 2.1.

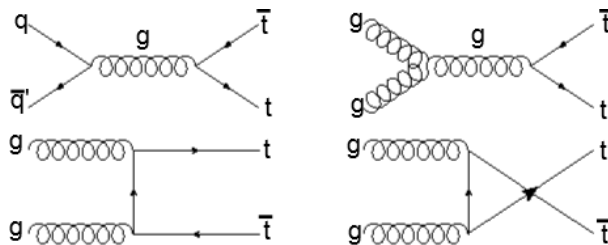


Figure 2.1: Leading order Feynman diagrams for top-antitop pair production via $q\bar{q}$ annihilation and gg fusion.

The partons inside the proton or antiproton carry only a fraction of the momentum the

2 Theoretical Fundamentals

hadrons carry themselves. The fraction of the momentum the partons carry is described by the so-called Bjorken- x . The effective centre-of-mass energy \hat{s} in a collision is given by

$$\hat{s} = x_1 x_2 s, \quad (2.7)$$

with x_i being the momentum fraction carried by the parton i and s the square of the centre-of-mass energy. To produce a top-antitop pair this effective centre-of-mass energy needs to be larger than two times the mass of the top quark, so $\sqrt{\hat{s}} \geq 2m_t$. This leads to the smallest possible Bjorken- x with a given centre-of-mass energy. If assumed that the fractions of both partons are equal, so $x_1 = x_2$, and if using a top mass of 173 GeV the smallest Bjorken- x for TEVATRON ($\sqrt{s} = 1.96$ TeV) and LHC ($\sqrt{s} = 8$ TeV) are

$$x \geq 0.18 \quad (\text{TEVATRON})$$

$$x \geq 0.04 \quad (\text{LHC}).$$

The fraction of antiquarks in protons is small because these particles are produced by vacuum fluctuations and are not the valence quarks in the proton. The probability to find partons at a given Bjorken- x is given by the parton distribution function (PDF) [19], which is a function of the Bjorken- x and the scale μ^2 at which they are evaluated. The PDF for two different μ^2 is shown in Figure 2.2. It is to see that the gluons are the most dominant partons at low Bjorken- x .

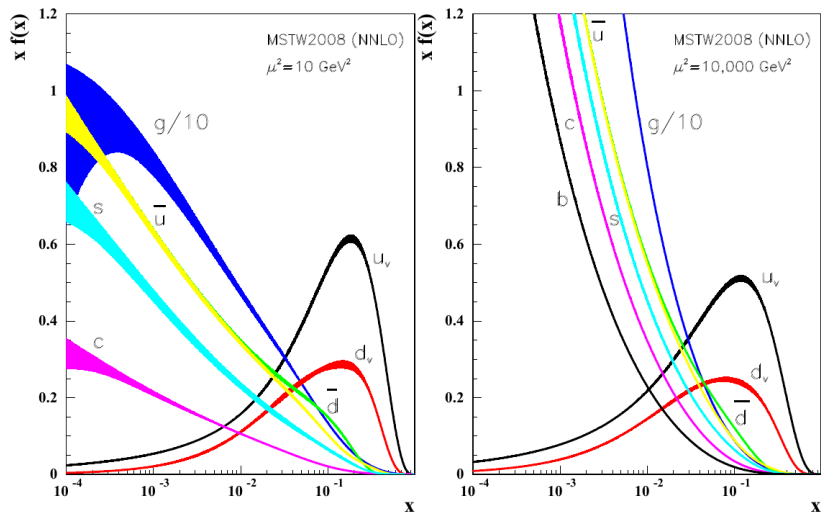


Figure 2.2: Parton distribution function for $\mu^2 = 10$ GeV (left) and $\mu^2 = 10,000$ GeV (right) [1].

Whether the $q\bar{q}$ annihilation or the gg fusion part is the dominant part depends on the hadrons used in the accelerator and the centre-of-mass energy. So at the TEVATRON, about 85% of the $t\bar{t}$ pair were produced by $q\bar{q}$ annihilation, while at LHC with $\sqrt{s} = 14$ TeV about 90% of the $t\bar{t}$ pair will be produced by gg fusion.

Single Top Production Another way to produce top quarks is by the electroweak interactions as single top quarks. For this process, the leading order Feynman diagrams are shown in Figure 2.3. This process has a smaller cross section than the $t\bar{t}$ production, but this process is more difficult to separate from the background because there are fewer particles and jets in the final state and hence the background is much larger. This process is very useful to measure the V_{tb} matrix element because the cross sections are directly proportional to the square of this matrix element. As mentioned before, this production was first observed 14 years after the discovery of the top quark.

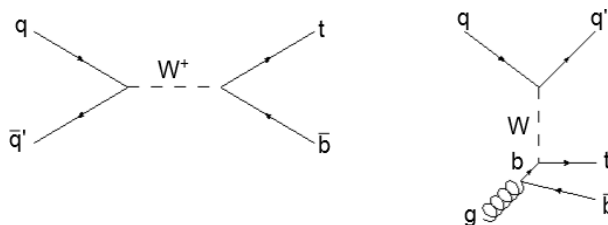


Figure 2.3: Leading order Feynman diagrams for single top production in s-channel (left) and t-channel (right).

2.2.3 Top Quark Decay

The top quark has a lifetime of about $\tau_t \approx 5 \cdot 10^{-25}$ s, so it is not possible to see a top quark in the detector, but just its decay products. Therefore it is necessary to know the decay channels of the top quark. As aforementioned, the top quark decays in the electroweak interaction $t \rightarrow Wq$, with q a down-type quark. This down-type quark is almost always a b quark, due to the V_{tb} matrix element. The total decay width is given in next-to-leading-order by the equation [18]

$$\Gamma_t = \frac{G_F m_t^3}{8\pi\sqrt{2}} \left(1 - \frac{m_W^2}{m_t^2}\right) \left(1 + 2\frac{m_W^2}{m_t^2}\right) \left(1 - \frac{2\alpha_s}{3\pi} \left[\frac{2\pi^2}{3} - \frac{5}{2}\right]\right), \quad (2.8)$$

with G_F the Fermi coupling and α_s the coupling of the strong interaction. This yields a decay width of $\Gamma_t \approx 1.35$ GeV [18] for a top mass of 173.3 GeV.

Neither the W boson nor the b quark are stable particles and will decay further. The b quark thereby has the property of decaying at a relatively far distance to the interaction

point. This makes it possible to identify this place as a secondary vertex with b -tagging. More about b -tagging is explained in Section 4.3. The b quark decays via the weak interaction and produces a jet via the strong interaction, which are called b jets, because of their origin.

The W boson has different decay channels and can decay hadronically into quarks, which form jets afterwards, or into a lepton and its related neutrino. In $t\bar{t}$ decays, there are three channels which are distinguished depending on the decay of the W bosons. The Feynman diagram for the decay in leading order is shown in Figure 2.4.

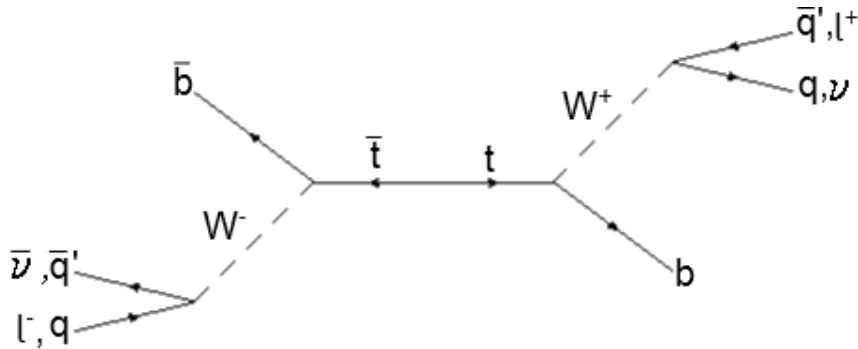


Figure 2.4: A Feynman diagram of a $t\bar{t}$ decay with possible finale states of the W boson.

All-jets Channel The first channel is the all-jets channel. In this channel both W bosons decay hadronically. This channel has the advantage that there is no missing transverse momentum, due to neutrinos, but the disadvantage that it is hard to distinguish between a top decay and multijet background, which also contains a lot of jets. This channel is, because of the colours of the quarks, the one with the highest branching ratio. The colours lead to a three times higher probability for quarks in the decay than to leptons because there are three different quarks the W can decay into.

Dilepton Channel Another possible decay channel is the dilepton channel. In this channel both W bosons decay into a lepton and its neutrino. The signature of this channel is composed of two different charged leptons and two b jets. Additionally, there is a high amount of missing transverse momentum, because of the two neutrinos that can not be detected. This channel is a very clean channel because of the low number of jets being produced and the two different charged leptons. The branching ratio of this decay is the smallest because there are no quarks produced.

Single Lepton Channel In the single lepton channel one of the two W bosons decays into a lepton and its neutrino, while the other one decays hadronically. The signature of

this channel is two b jets and two other jets, and one charged lepton with a high transverse momentum. This decay contains a neutrino, which carries momentum, but which can not be measured in the detector. But because there is only one neutrino, its momentum can be reconstructed by the missing transverse momentum.

The leptons used in this channel are only electrons and muons and not tau leptons that is just a convention because it is more difficult to identify tau leptons.

In the analysis in the later chapters, single-lepton events are used because of a good compromise between a good reconstruction and sufficient statistics.

3 Experimental Setup

3.1 Large Hadron Collider

The Large Hadron Collider (LHC) is a proton-proton collider at CERN in Geneva and nowadays the most powerful collider in the world. Next to proton-proton collisions at LHC there is the possibility to collide heavier lead ions. LHC is a synchrotron with a radius of about 27 km at approximately 100 m under the ground. It is placed in the tunnel where LEP, the Large Electron Positron Collider, was before. LHC started its operation in March 2010 with a centre-of-mass energy of 7 TeV. In 2012, the centre-of-mass energy was increased to 8 TeV and from spring 2013 until 2015 LHC has a scheduled downtime. For 2015 and the following years an operation at 13 TeV and 14 TeV is planned. The LHC was built for the search for the Higgs boson and new physics beyond the Standard Model. In 2012, the Higgs boson could be discovered, as mentioned in Section 2.1.3.

The LHC needs two beam pipes because both beams have the same charge, but need to be accelerated in different directions, so the particles can not be in the same pipe and the same magnetic dipole field. To force the particles with 7 TeV on a circular trajectory in a 27 km ring, the magnetic dipole field needs a strength of 8.33 T. Such a high magnetic field can not be reached by normal magnets. That is why superconducting magnets are needed. In the case of the LHC, the magnets are built with Nb-Ti, which are cooled with liquid helium to 1.9 K. To accelerate the particles inside the accelerator, superconducting radio frequency cavities are used. In addition, quadrupole magnets are used to focus the beams [20].

At maximum energy one beam contains 2808 bunches of protons, with 10^{11} protons in each bunch. The bunches cross all 25 ns.

At LHC, there are four major experiments with their detectors. These detectors are ALICE, ATLAS, CMS, and LHCb. ATLAS and CMS are multi-purpose detectors, while ALICE places a focus on lead ion collisions and LHCb focuses on physics with b quarks. The data used in the analysis is collected with the ATLAS detector, which will be explained in more detail in the next section.

3.2 The ATLAS Detector

ATLAS is an acronym for **A Torodial LHC ApparatuS**. It is a multi-purpose detector at the LHC. ATLAS is 44 m long covers 4π in solid angle with a diameter of 25 m and a weight of about 7,000 t. A sketch of the ATLAS detector with its components can be seen in Figure 3.1. The detector is composed of different sections, the inner detector, the calorimeter system, the muon spectrometer and the magnet system.

The coordinate system used by the ATLAS collaboration is a right-handed Cartesian coordinate system, with the origin set at the interaction point and the z axis pointing along the beam direction. The coordinates will be discussed in Chapter 4.5 in more detail.

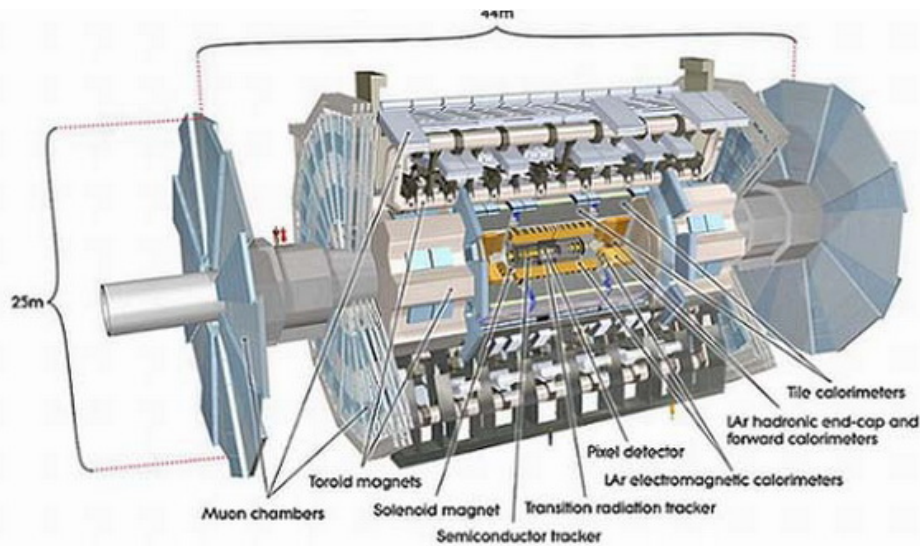


Figure 3.1: Cut-away view of the ATLAS detector [21].

3.2.1 Inner Detector

The inner detector consists of three different sub-detectors, these three are the Pixel detector, the Semiconductor Tracker (SCT) and the Transition Radiation Tracker (TRT). A solenoid with a length of 5.3 m and a diameter of 2.5 m surrounds the complete inner detector in a magnetic field of 2 T.

The Pixel detector and the SCT are used to distinguish between the interaction point and secondary vertices, for example for b -tagging purposes. The number of readout channels in the pixel detector is about 80.4 million and in the SCT about 6.3 million.

The TRT is used to determine the momentum of a particle by the curvature of the

particle's trajectory in the magnetic field, which is mainly used for $e - \pi$ separation. For this sub-detector, there are 315,000 readout channels [21].

3.2.2 Calorimeter System

The calorimeter is used to measure the energy of particles. This is done by depositing all of the particle's energy in the calorimeter. The particles do not leave the calorimeter afterwards. For the ATLAS detector, sampling calorimeters are used. A sampling calorimeter consists of active and passive material. The energy resolution can be approximated by

$$\frac{\sigma(E)}{E} = \frac{a}{\sqrt{E}} \oplus b, \quad (3.1)$$

where the first term depends on the material used for the calorimeter and the second one has to be added due to miscalibration, lost energy, etc. The \oplus means the quadrature summation of errors [22]. In ATLAS, there are two different calorimeters, the electromagnetic calorimeter and the hadronic calorimeter.

In the electromagnetic calorimeter, the energies of photons and electrons are measured. The processes of energy deposition are e^+e^- pair production and Bremsstrahlung. An electron, for example, enters the calorimeter and radiates Bremsstrahlung. The photon of the Bremsstrahlung then produces an e^+e^- pair, which radiates Bremsstrahlung again. By these processes a shower is formed in the calorimeter. The active material is liquid argon and the passive material is lead. The energy resolution of the electromagnetic calorimeter is roughly [23]

$$\frac{\sigma_E}{E} = \frac{10\%}{\sqrt{E}} \oplus 0.7\%. \quad (3.2)$$

The hadronic calorimeter is used to measure the energy of hadronic particles like protons. The passive material in this calorimeter is steel and scintillator the active one [21]. The energy resolution in this calorimeter is [23]

$$\frac{\sigma_E}{E} = \frac{50\%}{\sqrt{E}} \oplus 3\%. \quad (3.3)$$

3.2.3 Muon Spectrometer

The energy of muons can not be measured in the electromagnetic calorimeter because they do not radiate Bremsstrahlung and so they will not be stopped. For those muons, there

3 Experimental Setup

is an extra part in the outer layer of the detector. This part is the muon spectrometer. It consists of four different chambers, the Monitored Drift Tube (MDT), Cathode-Strip Chambers (CSC), Resistive Plate Chambers (RPC) and Thin Gap Chambers (TGC). The first two are used to measure the momenta of muons, while the other two are used as triggers. The muon spectrometer is immersed in an inhomogeneous toroidal magnetic field of 1 T to bend the trajectory of the muons to measure their momenta [21].

3.2.4 Trigger System

Everytime the beams cross, large amounts of data are provided, but most of the detected events are not appreciable. To select between interesting and not so interesting events, a trigger system is used. At the ATLAS detector, a *three-level trigger* system is used to identify interesting events. If the data would not be selected, it would be impossible to store all the data.

The first trigger is the level-1 trigger L1. It searches for high- p_T muons, electrons, photons, jets or hadronically decaying tau leptons and events with large transverse momentum and energy. The trigger makes fast decisions in about $2.5 \mu\text{s}$ and defines a region of interest (ROI). The level-2 trigger L2 checks the ROI and reconstructs the event. This trigger has a processing time of about 40 ms. The last trigger stage is the Event Filter EF that reconstructs and analyses the event with high precision algorithms, this takes about 4 s. After all three triggers the event is saved permanently.

4 Fundamentals of the Analysis

In the detector, just the final state products are observed, but not the initial particles. To figure out what particles were produced in the first place, the final state particles are compared with the signatures of the decay of interest. However, this signature is not unique due to other processes with the same end products, which are called background processes. To get better estimations of those background processes, Monte Carlo simulations of the signal and the background processes, are compared with the measured data. This comparison is often shown in graphical way in the form of control plots.

The observed decay channel of $t\bar{t}$ in this thesis is the single lepton channel, explained in Section 2.2.3. The signature of this channel consists of at least four jets, with two of them being tagged as b jets, a charged lepton, which is not a tau lepton, and a large amount of missing transverse momentum because of the neutrino in the final state. Several background processes have the same signature, they will be discussed in the following section.

4.1 Background Processes

The background processes for the single lepton $t\bar{t}$ decay are $W+$ jets and $Z+$ jets, as well as diboson processes with two weak bosons, so WW , ZZ and ZW events. Other background processes are single top decays and multijet events. Some of these processes contain a W boson which decays leptonically. These processes are the WW and ZW diboson background processes, the single top and the $W+$ jets background. The missing transverse momentum in these processes is caused by the neutrino from the leptonic W decay. In the multijet background, also called QCD background or misidentified lepton background, the lepton is faked by a jet and the missing transverse momentum comes from incomplete reconstruction of the jets or leptons. In the $Z+$ jets process, the Z decays into a lepton-antilepton pair, if one of them is not or incomplete detected, it seems like a $t\bar{t}$ decay, while the missing transverse momentum comes from the lepton, which could not be measured.

The $W+$ jets background is the most dominant background process. A possible Feynman

diagram for this process can be seen in Figure 4.1. Other Feynman diagrams for single top and dibosonic WW background events are shown in Figure 4.2.

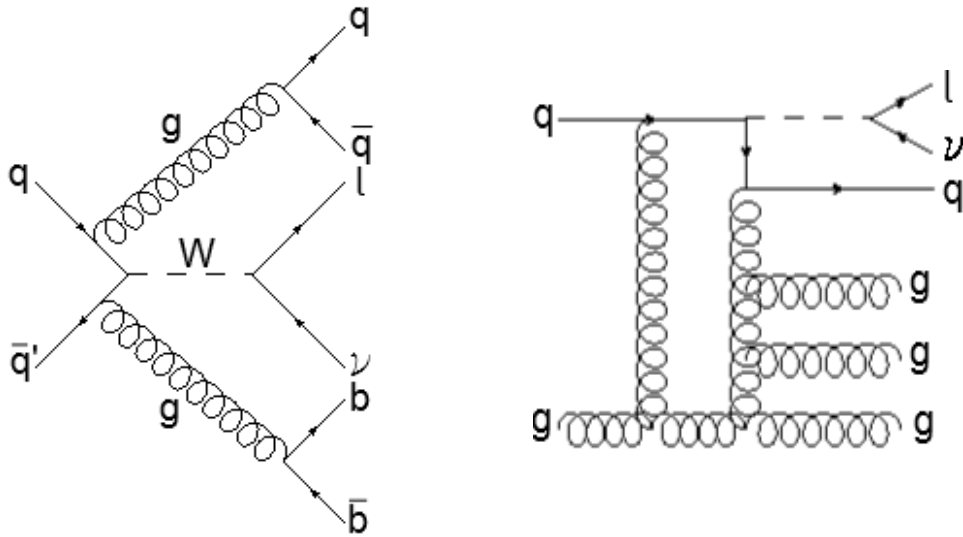


Figure 4.1: Two possible Feynman diagrams for a $W+$ jets background process with the signature of a $t\bar{t}$ decay.

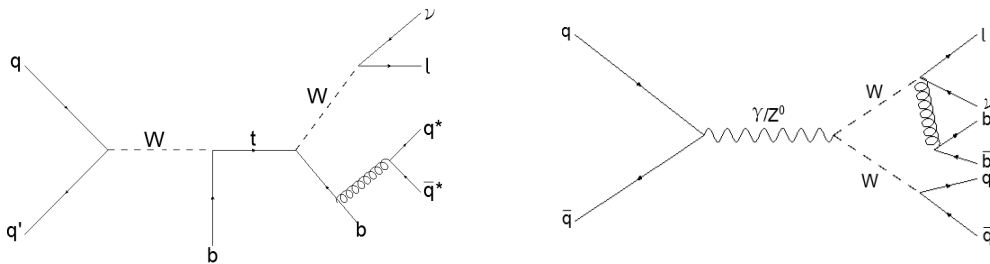


Figure 4.2: Possible Feynman diagrams for a single top (left) background and a WW (right) background process with the signature of a $t\bar{t}$ decay.

4.2 Simulated Events and Data Samples

The data samples used in the analysis are collected with the ATLAS detector, based on an integrated luminosity of $\int \mathcal{L} dt = 20.3 \text{ fb}^{-1}$ and at a centre-of-mass energy of $\sqrt{s} = 8 \text{ TeV}$. For better knowledge of the single processes, the signal process and background processes are produced by Monte Carlo generators, while for different processes there are different generator. These generators are thereby not only simulating the process itself, but also the detector. The simulation of the detector is done by GEANT 4 [24]. The simulated samples are afterwards handled like data received at the detector and are going through

the same analysis chain [25].

The simulated signal is produced with the Monte Carlo event generators POWHEG [26, 27] and PYTHIA [28]. The events for the $W+$ jets, $Z+$ jets and the diboson background are simulated by the generator ALPGEN [29] and PYTHIA. Some missing contributions in the dibosonic background are simulated with SHERPA [30]. The single top background is simulated, like the signal, with POWHEG and PYTHIA and events in the t-channel are generated by ACERMC [31] and PYTHIA.

The multijet background is not simulated by a Monte Carlo generator but estimated using the data. This estimation is done using a matrix method [32, 33].

4.3 *b*-Tagging

In the $t\bar{t}$ decay the two b jets are a very necessary part of the signature, because they are not that likely in background processes. Therefore it is very useful to have a good identification of these jets. As mentioned before, the b jets are identified by b -tagging. A jet out of other jets that is identified as a b jet is called tagged. The b quarks are forming mesons with other quarks, these mesons are B mesons. All these mesons containing a b quark have a comparatively long lifetime of a few ps [1]. The long lifetime is leading to a measureable flight length of a few millimetre and so to an observable secondary vertex [34]. A sketch of the idea of b -tagging can be found in Figure 4.3.

The easiest method of b -tagging is to call a jet a b jet if the impact parameter, defined as the distance between the interaction point and the point of closest approach, of a certain number of tracks is above a certain value.

In this analysis, the b -tagger is the MV1-tagger used at ATLAS. This tagger combines the information of three different high-performance taggers that use likelihood ratios. These three taggers are *IP3D*, *JetFitter* and *SV1*. The *IP3D* is an impact parameter based tagger using the significances of the impact parameter in longitudinal and transverse direction. The *JetFitter* finds a line which includes the interaction point and the secondary vertex. Finally, the *SV1* is based on the secondary vertices formed by B meson decays [34]. The MV1 is used with a weight of 0.7892, which corresponds to an efficiency working point of 70%.

4.4 D3PD

The Derived Physics Data (D3PD) are the data files used for analysis in ATLAS. These files are produced from the RAW data, which are the files received from the detector

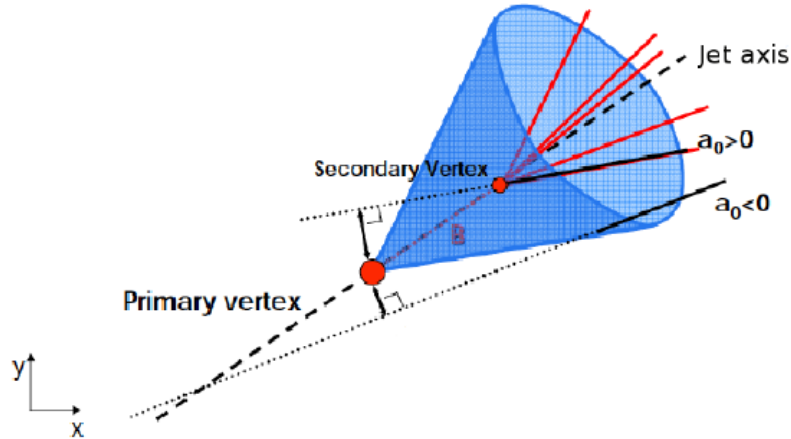


Figure 4.3: Sketch of a particle interaction with secondary vertex.

or the data from a Monte Carlo generator. The D3PD files contain as main part the information for each of the events in a TTree. Additionally, they include parameters of the beam like the bunch structure or the luminosity. In the D3PD files for MC data, there are additional information entries about the process, the so-called *truth*-information.

4.5 Kinematic Quantities

The analysis contains plots of quantities that are useful in particle physics. Those will be explained in this section. The quantities are based on the coordinates used at ATLAS, which is (ϕ, η, z) .

As aforementioned is z the direction that of the beam axis, ϕ is the azimuthal angle and defines the direction vertical to the beam axis. The quantity η is a parametrisation of the polar angle Θ and describes the angle between the flight direction and the beam axis. η is called pseudorapidity and depends on Θ according to

$$\eta = -\ln \tan \frac{\Theta}{2}. \quad (4.1)$$

The pseudorapidity is not Lorentz invariant, but pseudorapidity intervals are. Another advantage of η is that in inclusive QCD production, the intervals are containing almost the same number of particles.

Distances in the $\eta - \phi$ plane are called ΔR and are given by

$$\Delta R = \sqrt{\Delta\eta^2 + \Delta\phi^2}. \quad (4.2)$$

As mentioned in Section 2.2.2, the longitudinal momentum of a particle is unknown, but the transverse momentum p_T of the partons inside the hadron has to be 0, otherwise the particle would split apart. Due to momentum conservation, the transverse momentum after the interaction has to be 0 again. Therefore the transverse momentum is used to describe the motion of particles. A quantity linked to the transverse momentum is the missing transverse momentum \cancel{E}_T . This is the momentum that is missing to have a total momentum of 0. This momentum is carried by neutrinos and is used to describe their momentum.

In combination with the energy E or the mass M of a particle, p_T , η and ϕ are building an alternative four-vector that describes a particle.

5 TopRootCore

5.1 The Software Package TopRootCore

TopRootCore is a software package based on RootCore, which depends on Root. Root is an object-oriented programme, which was designed for data analysis in particle physics. It is written in C++ and was designed for the needs to analyse the data of the LHC [35]. RootCore is a software package used by the different groups at ATLAS to make the results easier to compare because not every group uses its own package. TopRootCore thereby is specified for the analysis needed for the top group. In TopRootCore, it is possible to implement additional packages depending on the analysis.

TopRootCore uses D3PD datasets, which are available for all ATLAS groups. There are D3PD datasets for Monte Carlo generated events and collision data. The data used for the analysis in Chapter 6 are the NTUP_TOP files. TopRootCore uses the D3PD files as input files and applies different event selections. Also estimations of the backgrounds and systematic uncertainties are performed. The output file is a Root file, which can be opened with Root.

In this analysis, the TopRootCore version 14-00-23 was used, which has several recommended cuts. Not included in this version are cuts on the missing transverse momentum and on the transverse mass of the W boson.

5.2 PlotFactory

The PlotFactory is a package implemented in TopRootCore. It was developed by the top group of the university in Göttingen. It uses the output files of TopRootCore and produces control plots. The PlotFactory package can be separated in two parts, the HistoCreator and the PlotFactory part itself. The HistoCreator takes the Root files, which are the output files of TopRootCore, and produces new Root files for different jet and b -tag options. The options are initialised in the Python script, which runs the HistoCreator. The chosen option for jets is the “4incl.”, what means that there are at least four jets. For the b -tags there are more possibilities, these are “0excl., 1excl., 2excl., 0incl., 1incl.” and

“2incl.”, while exclusive means that there are exactly 0, 1 or 2 jets with a MV1 weight larger than 0.7892 and which means they are tagged as b jets. For the inclusive option, there are more than 0, 1 or 2 jets tagged as b jets.

The analysis of the data is also done in the HistoCreator, while these analyses are done in external files to give a better overview of the single analysis steps. The different files make it easier to modify or add single analysis steps.

The quantities for the analysis are saved in TH1D histograms and depending on their origin, saved in different Root files and different folders, which contain information of the number of jets and the number of b -tags. Additionally, the Python script has the option of activating or deactivating single background processes, for example, to give the possibility to run the programme faster to see changes in the output files.

The PlotFactory takes the output files of the HistoCreator and fills their information into control plots. There are control plots for different b -tag options and also for the two lepton possibilities, so electrons or muons. In addition to the control plots, the PlotFactory produces an HTML file, where all plots are presented. Again, there are two different HTML files for the same b -tag options, one for the electron channel and one for the muon channel. Next to the plots, the HTML files contain the event yield tables, where the numbers of events for the data, simulated signal and the different background processes are shown. These numbers are calculated by summing the bin contents of the single bins for a process in the Root files produced by the HistoCreator.

The control plots show the different simulated processes as coloured boxes and produces a Root object, called stack, of these boxes by batching them on each other. The detector data is included as points. Additionally to the information of the processes, parameters of the detector like the integrated luminosity $\int \mathcal{L} dt$ are included, as well as a legend containing the colour code, explaining which colour belongs to which process.

6 Results

This bachelor project was to modify the PlotFactory package implemented in TopRootCore as introduced in Section 5.2. There were four major modifications added to the PlotFactory package. These changes were to renew the HTML page produced by the PlotFactory to present the plots in a clearer way. The implementation of plots for *Pseudo Top* related distributions. Another project was to add goodness-of-fit tests, the χ^2 and Kolmogorow-Smirnow tests to the analysis and displayed them in the plots. Another modification was to produce a plot with logarithmic y axis for all quantities. The changes are applied for the group project of measuring the decay width of the top quark. Also, the progress of the group project will be displayed.

During the project, a discrepancy in the selected events could be observed. The progress of improving this discrepancy will be shown, however, investigating the reasons for the discrepancy is not part of this analysis. The displayed plots in the analysis are for the electron channel, for reasons of completeness some muon plots are included in Appendix A. To compare the results with results of other groups, additional cuts were applied to the analysis. These cuts were applied on the missing transverse momentum and the transverse mass of the W boson. The missing transverse momentum cut is $\cancel{E}_T > 30$ GeV and the transverse mass cut $M_T > 30$ GeV. For the same reason another b -tag calibration was used. In addition to the b -tag calibration recommended in TopRootCore, *System8* [36], the calibration method *default* was tested. Exemplary control plots for the different b -tag calibration options can be seen in Figure 6.1. The *System8* method uses three selection criteria, which are uncorrelated to a data sample with a muon associated with a jet to build a system of eight equations to serve as calibration for the b -tagger. The *default* method uses $t\bar{t}$ events to calibrate the b -tagger. The plots show the p_T values of the jet with the highest p_T in each event. If not mentioned otherwise, for all plots the *System8* calibration was used.

6 Results

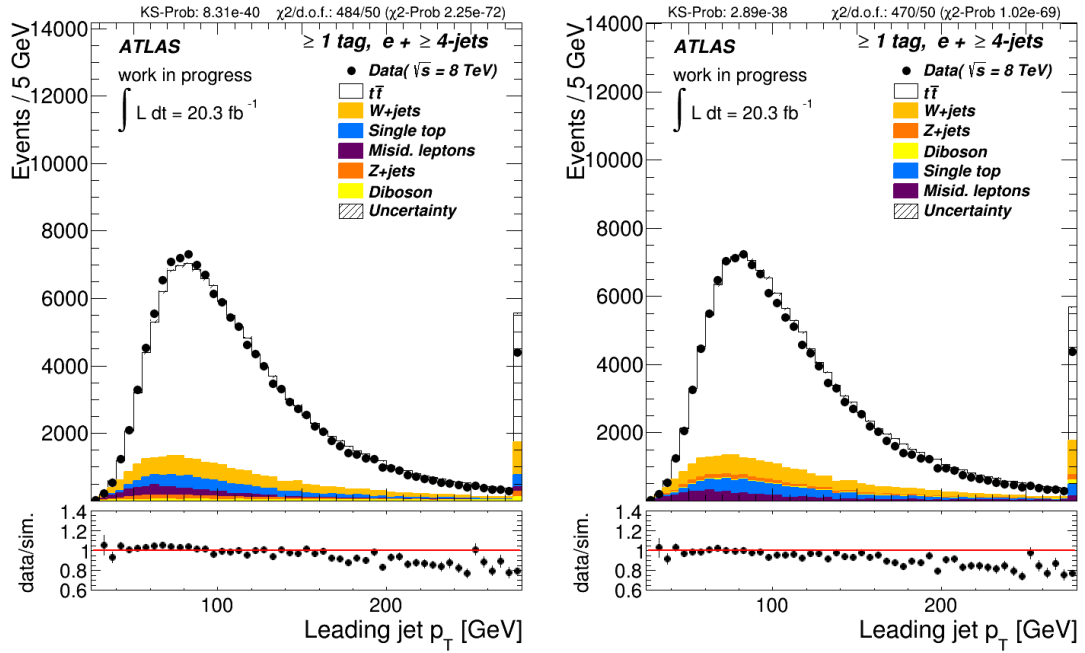


Figure 6.1: Control plots of the p_T values of the jet with the highest p_T , with electron as lepton in events with ≥ 1 b -tagged jet, for the different b -tag calibrations *System8* (left) and *default* (right) without the event reweighting.

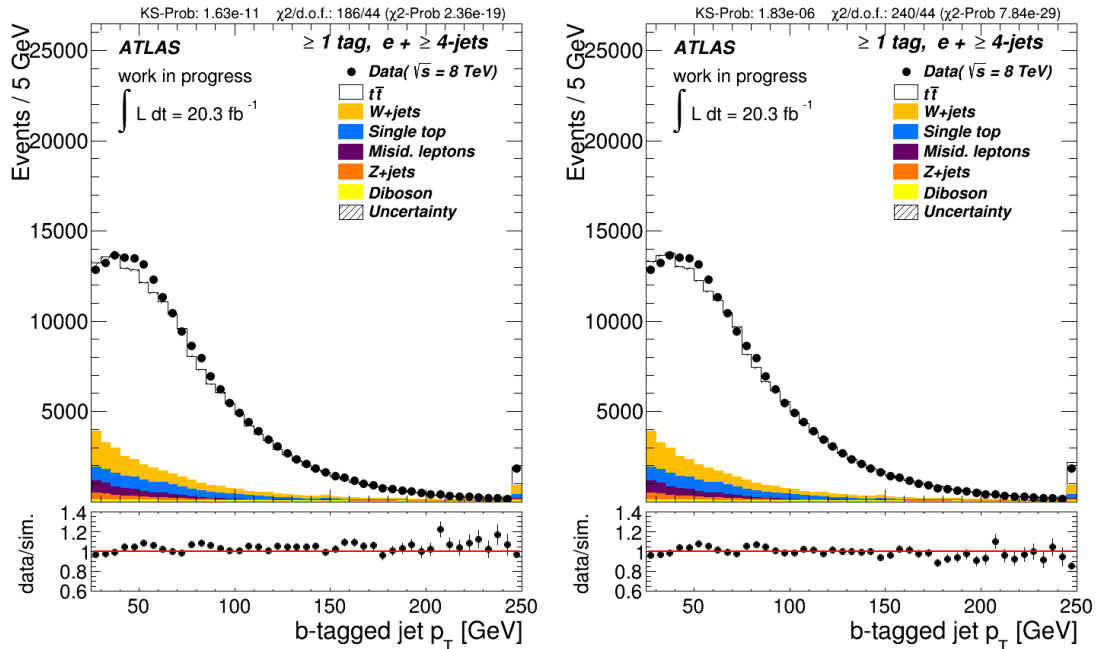


Figure 6.2: Control plots of the p_T values of the jets tagged as b jets, with electron as lepton in events with ≥ 1 b -tagged jet, for reweighted (left) and not reweighted (right) samples.

| Process | Selected Events | |
|---------------|------------------|--------------|
| | Electron Channel | Muon Channel |
| $t\bar{t}$ | 106,836 | 164,826 |
| Single Top | 7,649 | 11,811 |
| W +jets | 14,314 | 24,920 |
| Z +jets | 2,573 | 2,822 |
| Diboson | 886 | 1,358 |
| Misid. lepton | 4,189 | 4,866 |
| Total | 136,450 | 210,606 |
| Data | 136,518 | 221,824 |

Table 6.1: Event yield table for events with a setting using ≥ 4 jets and ≥ 1 b -tag jet after the applied reweighting.

The $t\bar{t}$ data sample was additionally reweighted, because the sample used for signal overshoots the data for high p_T of the top and antitop. The difference between the reweighted $t\bar{t}$ sample and the not reweighted events can be seen in Figures 6.2, additionally, the event yield tables after the reweighting can be seen in Table 6.1 for the electron and muon channel. In these plots, the p_T of the b -tagged jets is shown, as an example. The ratio plot shows that the fluctuations get less and only appear in sections with low statistics, like the tail of the distribution. These plots are made with the four jet inclusive and one b -tag inclusive option because of the higher statistics in this channel and also these settings are also the ATLAS recommended ones, so it makes comparisons with results of different groups easier.

In addition, further plots for b -tag exclusive options were made, to see the effect on the background processes and to check, if the programme works properly for all available b -tag options. In Figure 6.3 the options “2excl.” and “0excl.” are compared. As expected, nearly no $t\bar{t}$ events are left for the “0excl.”, as they have two b -tagged jets, which both have to be miss-detected, to pass the “0excl.” event selection. For the “2excl.” events, there is a much less background, that can be explained because these processes need to have two b -tagged jets, which is not likely for background processes.

6.1 HTML Page

In order to have all the plots in a clearly arranged way, the PlotFactory has the feature of producing an HTML file where all the plots are presented. This makes it also easier to take a look at the different control plots. A part of the bachelor project was to modify the HTML page. The original HTML page presented all the plots among one another, this

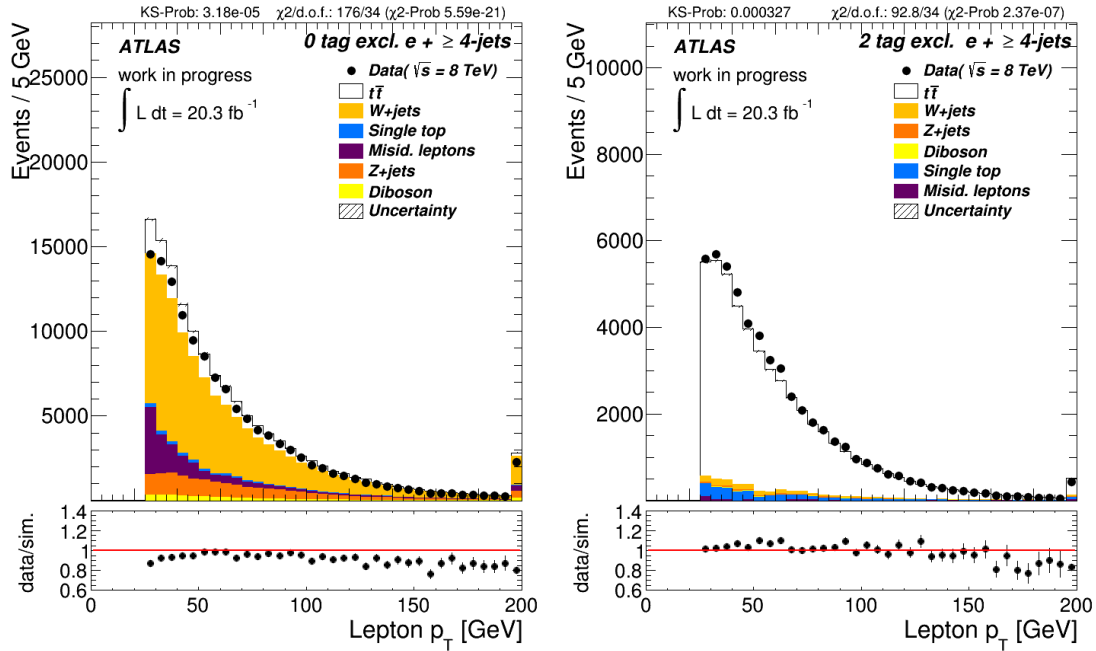


Figure 6.3: Control plots of the p_T values of electrons in events with exactly 0 (left) and 2 (right) b -tagged jet with reweighted samples.

was changed to have a control plot with a linear y axis beside the corresponding control plot with the logarithmic y axis. This gives a nice overview of the quantity presented in the plot.

Additionally, the HTML page shows the event yield for the examined lepton type and number of b -tags. This is retained, but for the event yield an additional HTML is produced, where just the event yield is included. Also, not only the event yield table for the lepton type in the plots is shown, but also the event yield of the other lepton type by the same b -tag setting. This was useful especially to check the event yields, when the different b -tagging calibrations and the $t\bar{t}$ reweighting method were tested, to the differences in the muon channel and the electron channel.

For a faster navigation between the single lepton types and b -tag settings, a navigation bar was implemented, where the different lepton types and b -tag settings can be selected. A Screenshot of the navigation bar and the event yield tables can be seen in Figure 6.4.

6.2 Pseudo Top Distributions

The pseudo top distributions are necessary for unfolding studies, where the potential of separating the distribution of the top quark mass and the smearing caused by the detector is tested. If it is possible to separate these two distributions, the detector effects can be

Electron:
• 0Inclusive 1Inclusive 2Inclusive 0Exclusive 1Exclusive 2Exclusive

Muon:
• 0Inclusive 1Inclusive 2Inclusive 0Exclusive 1Exclusive 2Exclusive

| Event Yield Electron Channel | | Event Yield Muon Channel | |
|------------------------------|---------|--------------------------|---------|
| TTbar | 106836 | TTbar | 164826 |
| Single Top | 7649.91 | Single Top | 11811.6 |
| W+jets | 14314.9 | W+jets | 24920.3 |
| Z+jets | 2573.06 | Z+jets | 2822.84 |
| Diboson | 886.28 | Diboson | 1358.76 |
| Misid. lepton | 4189.36 | Misid. lepton | 4866.98 |
| Total | 136450 | Total | 210606 |
| Data | 136518 | Data | 221824 |

Figure 6.4: Screenshot of the navigation bar and the event yield as they are presented in the HTML file.

subtracted from the data and the pure top distribution is observable, where the decay width of the top quark can be measured and as mentioned before, that would lead to a precision measurement of the lifetime of the top quark.

Pseudo top quarks are objects which are constructed in events with at least four jets and at least two of them tagged as b jets, so the recommended settings with at least four jets and at least one b jet is not useful here. Instead, the “2incl.” b -tag option is used. The algorithm to build pseudo top quarks is the following:

- the two b -tagged jets are supposed to be coming directly from the pseudo top, if there are more than two, the one with the most p_T are chosen.
- the two jets with highest p_T that are not the b -tagged jets from the pseudo top are combined as the pseudo W .
- the b jet with the smaller ΔR related to the lepton is supposed to be from the leptonically decaying pseudo top while the other from the hadronically decaying pseudo top.
- the hadronically decaying pseudo top can be constructed with the pseudo W and the related b jet, while the leptonically decaying one is not possible to be constructed because the four vector of the neutrino is not completely known.

The objects are called pseudo top quarks because it is not clear that the constructed particles are really the top quarks. For each $t\bar{t}$ event, only one pseudo top can be constructed,

6 Results

because the neutrino can not be fully reconstructed without making conclusions on the result. A possible way to reconstruct the neutrino would be to force the sum of the lepton and the neutrino to build an object with the mass of the W boson.

The results of these analyses are shown in Figure 6.5, where it can be seen that the peak of the mass is near the value of the mass of the top quark. In addition, the control plots of the p_T and mass of the hadronically decaying pseudo W boson, which can also be constructed, are shown in Figure 6.6. Also in this plots, it can be seen that the mass peak is at the expected place, so close to the mass of the W boson.

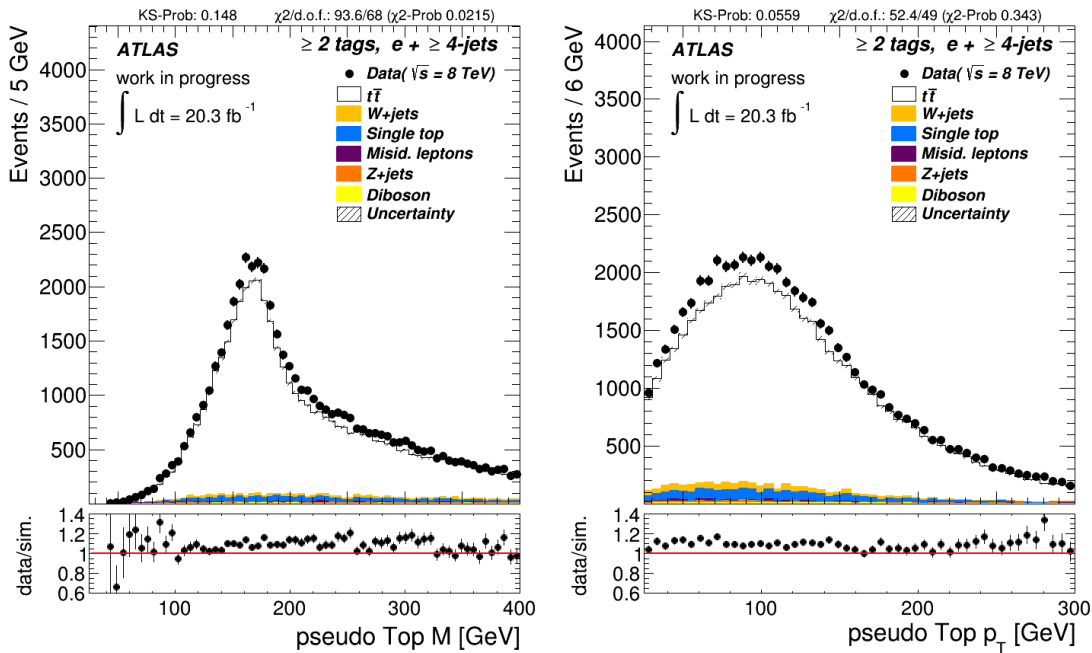


Figure 6.5: Control plots of the mass (left) values and the p_T (right) of pseudo top quarks in events with electrons as lepton and ≥ 2 b -tagged jets in reweighted samples.

6.3 Goodness-of-Fit Test

For a comparison of data taken by a detector quantify data produced by a Monte Carlo generator, it is necessary to have methods to proof their agreement. This is accomplished by goodness-of-fit tests which compare for example data points with a regression function or in this case simulated data. There are a lot of different goodness-of-fit tests and two of them were implemented in the PlotFactory, in this bachelor project. These two are the Kolmogorow-Smirnow (K-S) test and the χ^2 test. For both, a short explanation will be given later in this section. The χ^2 test is implemented as a comparison of an unweighted

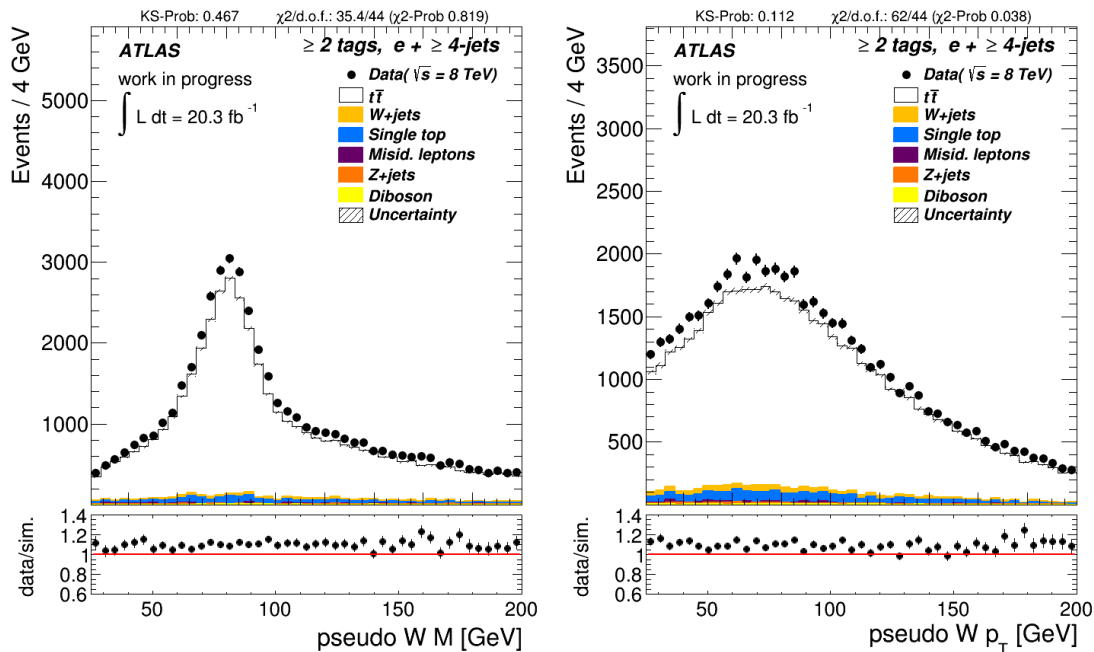


Figure 6.6: Control plots of the mass (left) values and the p_T (right) of pseudo W boson in events with electrons as lepton and ≥ 2 b -tagged jets in reweighted samples.

histogram, which corresponds to the data from the detector and a weighted histogram, which corresponds to the Monte Carlo events. The results for both of the tests can be seen at the top of every plot. For the K-S test the p -value is displayed and for the χ^2 test the χ^2 value over the degrees of freedom and also the χ^2 probability. The worst possible result for the probability is 0 and the best 1.

6.3.1 χ^2 Test

In a histogram with M bins, assuming the fluctuations in each bin are independent, the χ^2 value can be calculated as

$$\chi^2 = \sum_{i=1}^M \frac{(n_i - v_i)^2}{V[v_i]}, \quad (6.1)$$

with n_i the number of events predicted by the Monte Carlo events in bin i and v_i the number of events in the detector data in bin i and $V[v_i]$ the variance. For a perfect agreement, it's $\chi^2/\text{d.o.f.}=1$, with d.o.f the degrees of freedom, the value increases for worse agreements in the histograms. The χ^2 probability is the probability that a measurement give an χ^2 value which is equal to or larger than the obtained one [37].

6.3.2 Kolmogorow-Smirnow Test

The K-S test is based on an empirical cumulative distribution function $F_N(x)$, with N the number of measurements of an observable. This can be compared with another cumulative distribution function $F(x)$. The largest distance between these two function D_N is given by

$$D_N = \max|F_N(x) - F(x)|. \quad (6.2)$$

The value $\sqrt{N}D_N$ defines the critical region for the K-S test, for a perfect agreement applies $D_N = 0$ and increases for less agreement. The K-S test can also be used for data with low statistics [37].

6.4 Logarithmic Scale Plots

In regions with low statistics and backgrounds, which are not as likely, the visibility is very low. To amplify the visibility, it is necessary to add plots with a logarithmic y axis, so that no details are overlooked. The used logarithm is the one to the base 10. For the maximal value on the y axis a high value was chosen to avoid the histograms overlap with the legend, so the histograms and the legend are still readable without problems. The minimal value was chosen by taking the smallest background and for this smallest background the smallest entry while still being larger than 0. Because of the weighting of the generated processes, this value can be smaller than 1. If the smallest entry is found, the minimum for the y axis is the order of this value minus one. This way, the minimum is not chosen arbitrarily. An example for a plot with logarithmic scale and the advantage for regions with low statistics can be seen in Figure 6.7 in plots with the p_T values for all jets, because this quantity has a long tail.

In the plots themselves, the backgrounds are sorted by the number of events they have in the 4 jets inclusive and 1 b jet inclusive setting. So the dibosonic background, which has the least number of events, is at the bottom of the plot, above is the $Z+$ jets background. On top of them is the multijet background, followed by the single top background and the background with the most events is $W+$ jets background, which is at the top of the coloured histograms.

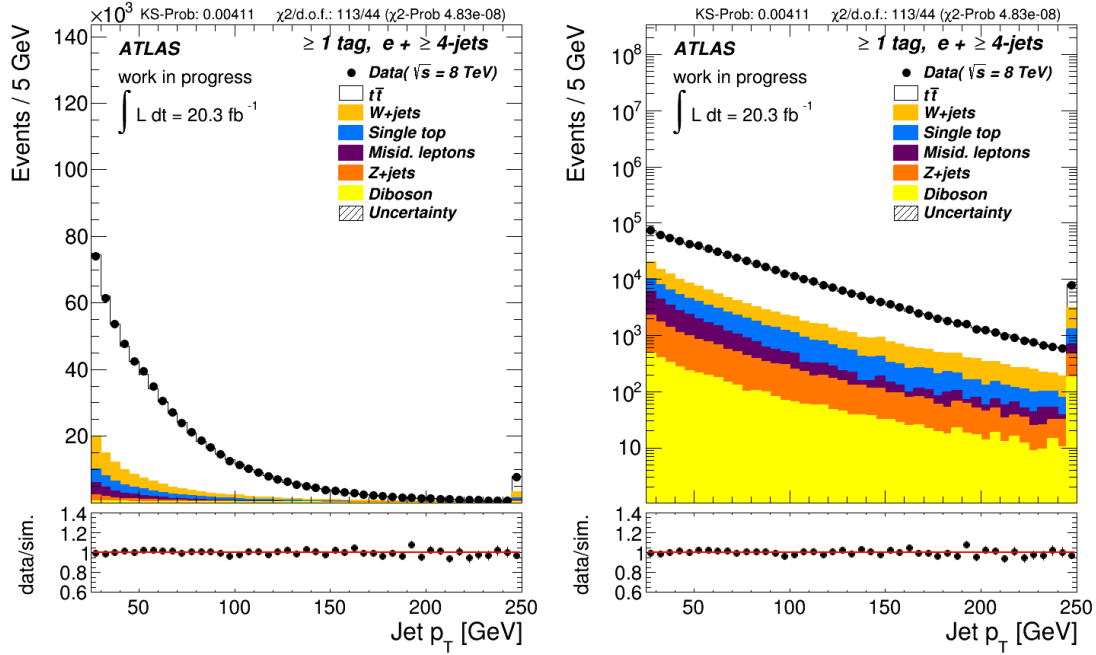


Figure 6.7: Control plots for the p_T values of all jets with normal linear y axis (left) and logarithmic y axis (right) in events with electrons as lepton and ≥ 1 b -tagged jet in reweighted samples.

6.5 Modifications of the Layout

During the project, different modifications on the layout of the control plots have been made. These were, for example, to change the legend that way that the events are displayed in the order they have in the plots. Also, the value of the integrated luminosity was set to the current value and the x axis label of the plots showing the number of jets and the number of b -tagged jets. The changes in the axis labels were to illustrate that the last bin contains additionally the overflow bin and so, not just the events with 7 jet or 3 b -tagged jets. The plots for the number of jets and the number of b -tagged jets can be seen in Figure 6.8.

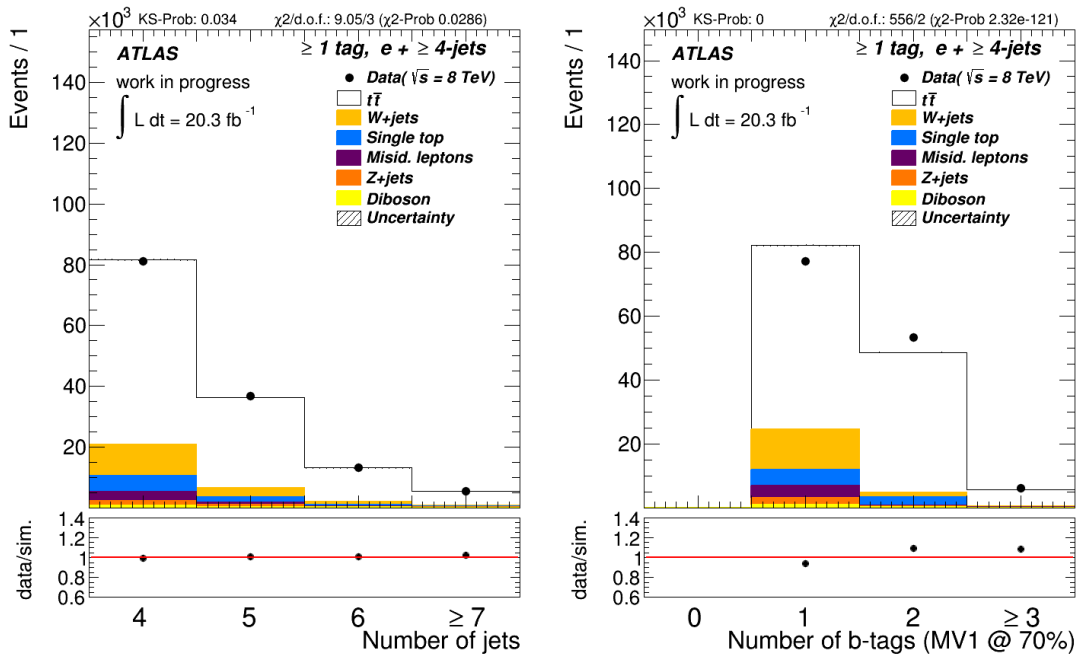


Figure 6.8: Control plots for the number of jets (left) and the number of b -tagged jets (right) in events with electrons as lepton and ≥ 1 b -tagged jet in reweighted samples.

7 Conclusion

The main part of the bachelor project was to modify the PlotFactory package, which is implemented in TopRootCore and is used to produce control plots. The modifications done included a renewed HTML page that now contains additional information and plots that are arranged in a clearer way. Also, the navigation between the different lepton types and b -tag settings has been improved.

The pseudo top construction included in the analysis, shows a peak near the mass of the top quark and also the pseudo W mass peak is in the expected region. So these results can be used for additional studies to measure the decay width of the top quark.

The logarithmic scales simplify observations of smaller backgrounds and in regions with low statistics so that nothing is overlooked.

The goodness-of-fit tests make it possible to see if there is a good comparison between the data recorded at the detector and the events produced with Monte Carlo generators, without the subjective component of judging the agreement by eye.

During the studies, several smaller bugs inside the PlotFactory package were found and fixed, even apart from the modified parts of the programme.

The PlotFactory produces and presents the control plots now in a clearer way.

A Additional Plots

A Additional Plots

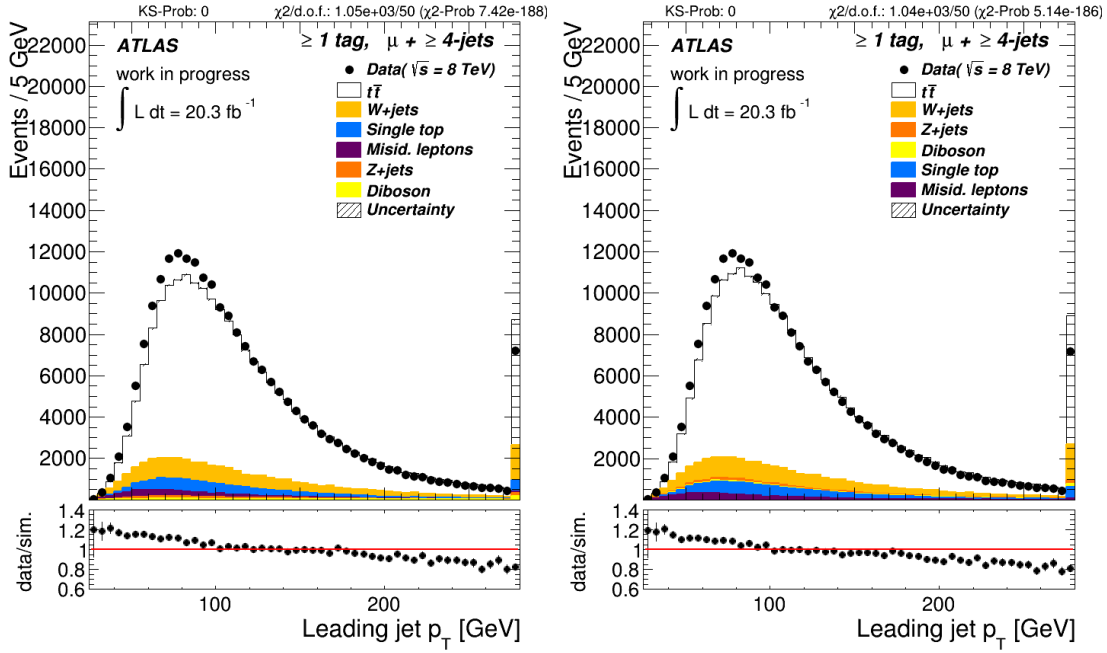


Figure A.1: Control plots of the p_T values of the jet with the highest p_T , for muon in events with ≥ 1 b -tagged jet, for the different b -tag calibrations *System8* (left) and *default* (right) without the event reweight.

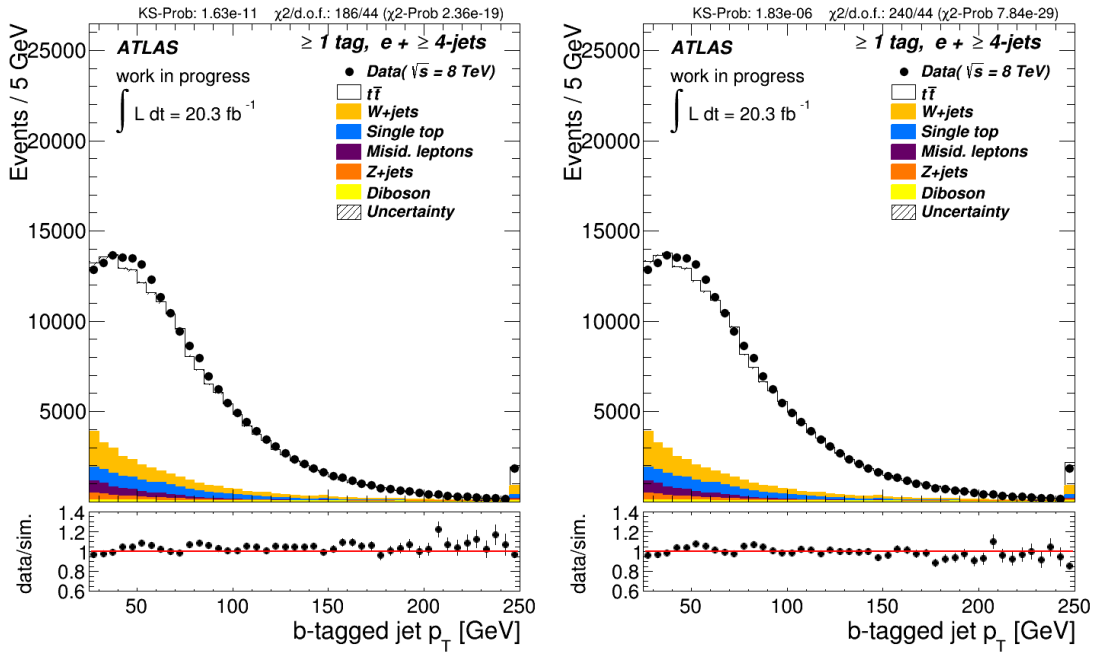


Figure A.2: Control plots of the p_T values of the jets tagged as b jets, with muons as lepton in events with ≥ 1 b -tagged jet, for reweighted (left) and not reweighted (right) samples.

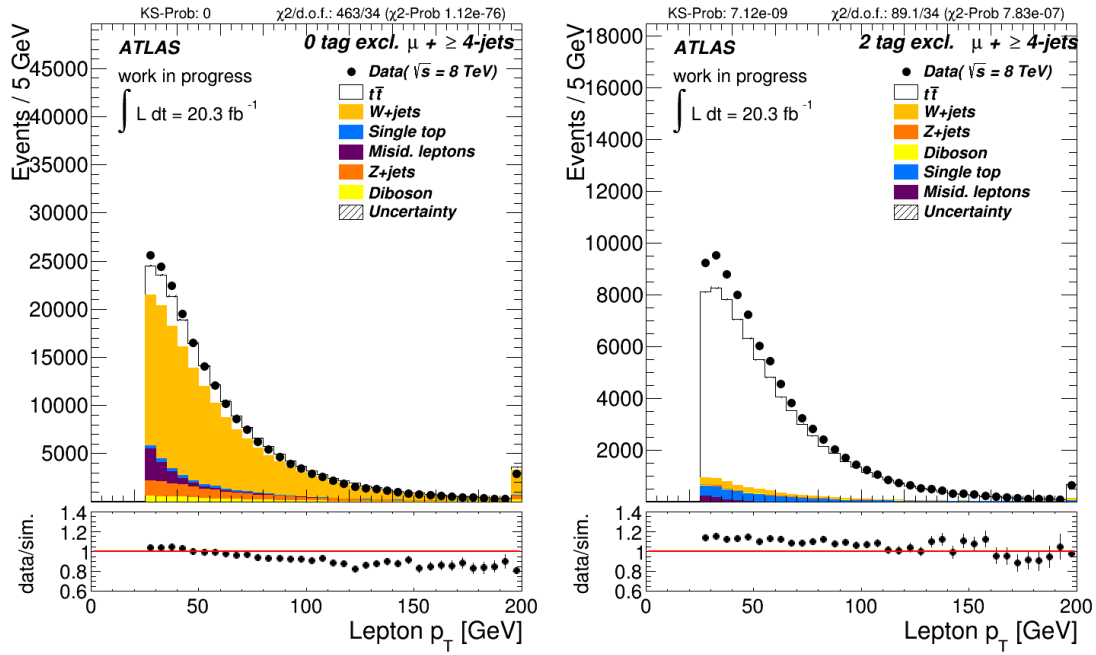


Figure A.3: Control plots of the p_T values of muons in events with exactly 0 (left) and 2 (right) b -tagged jet with reweighted samples.

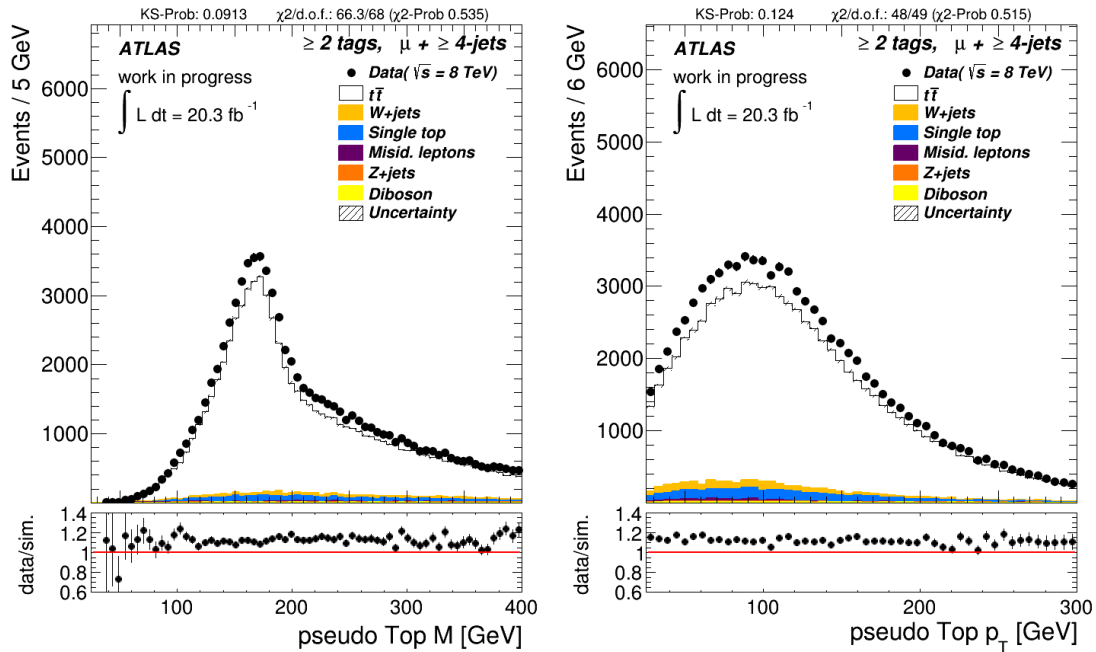


Figure A.4: Control plots of the mass (left) values and the p_T (right) of pseudo top quarks in events with muons as lepton and ≥ 2 b -tagged jets in reweighted samples.

A Additional Plots

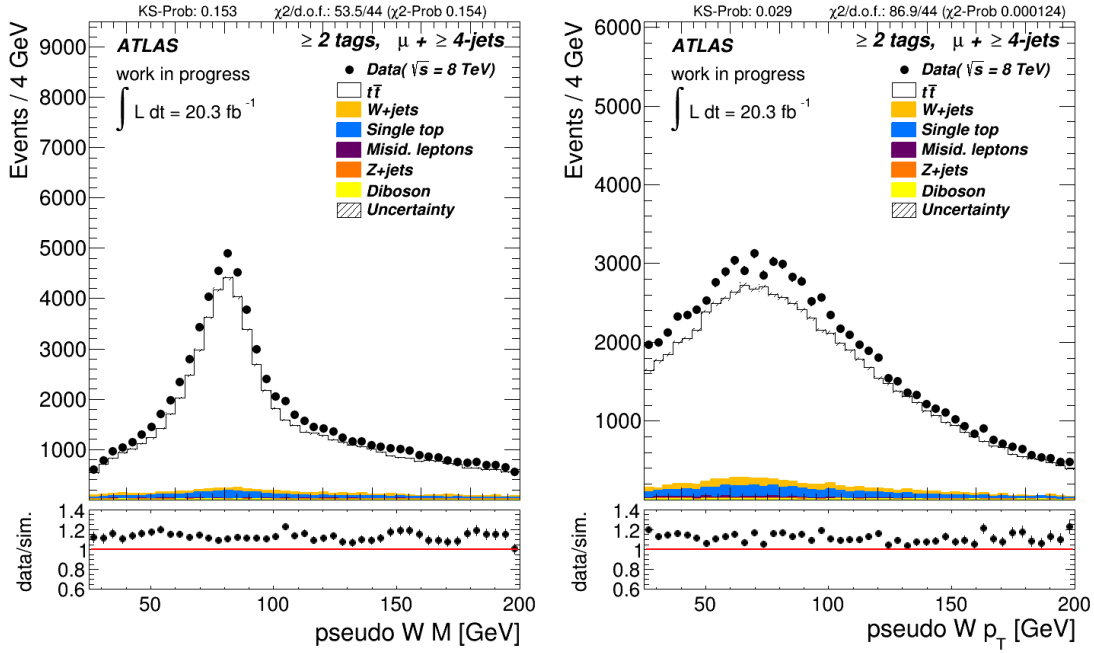


Figure A.5: Control plots of the mass (left) values and the p_T (right) of pseudo W boson in events with muons as lepton and ≥ 2 b -tagged jets in reweighted samples.

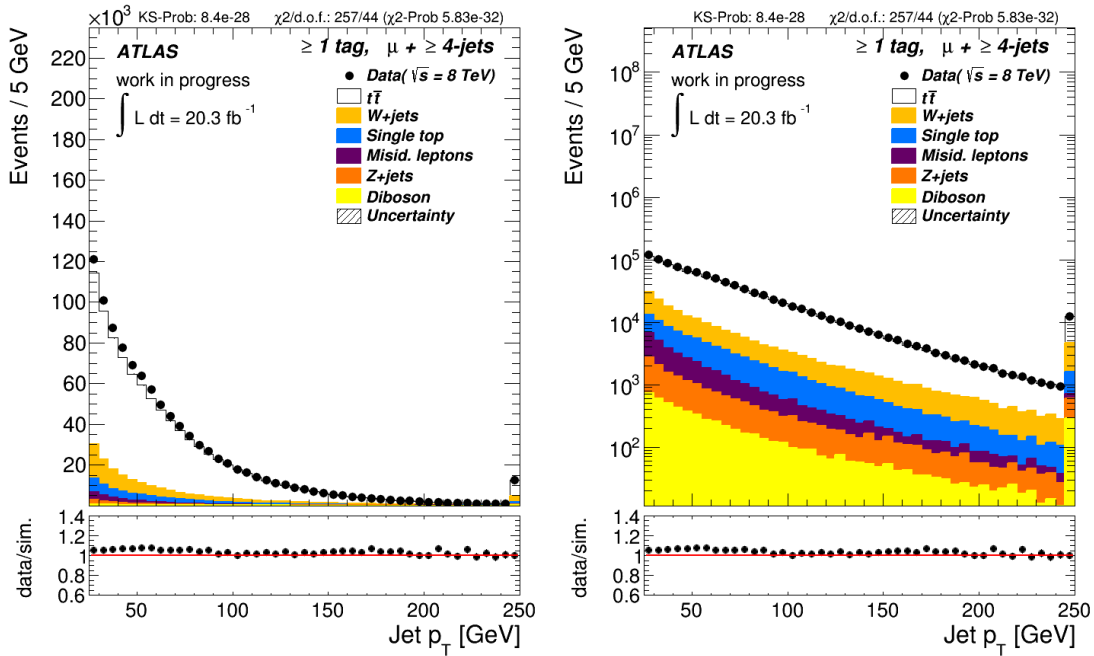


Figure A.6: Control plots for the p_T values of all jets with normal linear y axis (left) and logarithmic y axis (right) in events with muons as lepton and ≥ 1 b -tagged jet in reweighted samples.

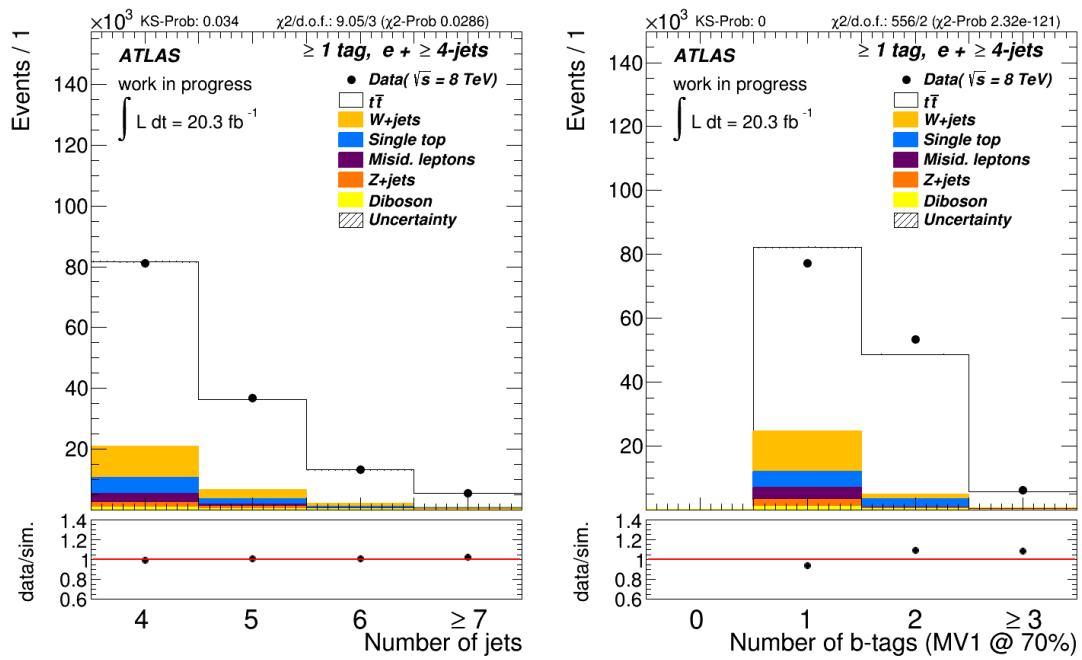


Figure A.7: Control plots for the number of jets (left) and the number of b -tagged jets (right) in events with muons as lepton and ≥ 1 b -tagged jet in reweighted samples.

Bibliography

- [1] J. Beringer, et al. (Particle Data Group), *Review of Particle Physics*, Phys. Rev. D **86**, 010001 (2012)
- [2] M. Kobayashi, T. Maskawa, *CP Violation in the Renormalizable Theory of Weak Interaction*, Prog. Theor. Phys. **49**, 652 (1973)
- [3] N. Cabibbo, *Unitary Symmetry and Leptonic Decays*, Phys. Rev. Lett. **10**, 531 (1963)
- [4] S. Glashow, *Partial Symmetries of Weak Interactions*, Nucl. Phys. **22**, 579 (1961)
- [5] A. Salam, J. C. Ward, *Weak and electromagnetic interactions*, Nuovo Cim. **11**, 568 (1959)
- [6] S. Weinberg, *A Model of Leptons*, Phys. Rev. Lett. **19**, 1264 (1967)
- [7] P. W. Higgs, *Broken Symmetries and the Masses of Gauge Bosons*, Phys. Rev. Lett. **13**, 508 (1964)
- [8] F. Englert, R. Brout, *Broken Symmetry and the Mass of Gauge Vector Mesons*, Phys. Rev. Lett. **13**, 321 (1964)
- [9] G. Guralnik, C. Hagen, T. Kibble, *Global Conservation Laws and Massless Particles*, Phys. Rev. Lett. **13**, 585 (1964)
- [10] ATLAS Collaboration (G. Aad, et al.), *Observation of a new particle in the search for the Standard Model Higgs boson with the ATLAS detector at the LHC*, Phys. Lett. **B716**, 1 (2012)
- [11] CMS Collaboration, *Observation of a new boson at a mass of 125 GeV with the CMS experiment at the LHC*, Phys. Lett. **B716**, 30 (2012)
- [12] CDF Collaboration (T. Aaltonen, et al.), *Observation of top quark production in $\bar{p}p$ collisions*, Phys. Rev. Lett. **74**, 2626 (1995)

Bibliography

- [13] DØ Collaboration (V.M. Abazov, et al.), *Observation of the top quark*, Phys. Rev. Lett. **74**, 2632 (1995)
- [14] CDF Collaboration (T. Aaltonen, et al.), *First Observation of Electroweak Single Top Quark Production*, Phys. Rev. Lett. **103**, 092002 (2009)
- [15] DØ Collaboration (V.M. Abazov, et al.), *Observation of Single Top Quark Production*, Phys. Rev. Lett. **103**, 092001 (2009)
- [16] ATLAS Collaboration (G. Aad, et al.), *Measurement of the top quark charge in pp collisions at $\sqrt{s} = 7$ TeV with the ATLAS detector*, JHEP **1311**, 031 (2013)
- [17] ATLAS Collaboration, CDF Collaboration, CMS Collaboration, DØ Collaboration, *First combination of Tevatron and LHC measurements of the top-quark mass*, ATLAS-CONF-2014-008, CDF-NOTE-11071, CMS-PAS-TOP-13-014, DØ-NOTE-6416 (2014)
- [18] T. Liss, A. Quadt (Particle Data Group), *Review of Particle Physics: The Top Quark*, Phys. Rev. D **86**, 010001 (2012)
- [19] J. Pumplin, et al., *New generation of parton distributions with uncertainties from global QCD analysis*, JHEP **0207**, 012 (2002)
- [20] O. S. Bruning, et al., *LHC Design Report. 1. The LHC Main Ring*, CERN-2004-003-V-1, CERN-2004-003 (2004)
- [21] ATLAS Collaboration (G. Aad, et al.), *The ATLAS Experiment at the CERN Large Hadron Collider*, JINST **3**, S08003 (2008)
- [22] C. Berger, *Elementarteilchenphysik: Von den Grundlagen zu den modernen Experimenten*, Springer-Lehrbuch, Springer (2006)
- [23] ATLAS Collaboration (G. Aad, et al.), *ATLAS: Detector and physics performance technical design report. Volume 1*, CERN (1999)
- [24] S. Agostinelli, et al. (GEANT4), *GEANT4: A Simulation toolkit*, Nucl. Instrum. Meth. **A506**, 250 (2003)
- [25] ATLAS Collaboration (G. Aad, et al.), *The ATLAS Simulation Infrastructure*, Eur. Phys. J. **C70**, 823 (2010)

- [26] G. Corcella, et al., *HERWIG 6.5 release note*, CAVENDISH-HEP-02-17, DAMTP-2002-124, KEK-TH-850, MPI-PHT-2002-55, CERN-TH-2002-270, IPPP-02-58, MC-TH-2002-7 (2002)
- [27] G. Corcella, et al., *HERWIG 6: An Event generator for hadron emission reactions with interfering gluons (including supersymmetric processes)*, JHEP **0101**, 010 (2001)
- [28] T. Sjostrand, et al., *PYTHIA 6.4 Physics and Manual*, JHEP **0605**, 026 (2006)
- [29] M. L. Mangano, et al., *ALPGEN, a generator for hard multiparton processes in hadronic collisions*, JHEP **0307**, 001 (2003)
- [30] T. Gleisberg, et al., *Event generation with SHERPA 1.1*, JHEP **0902**, 007 (2009)
- [31] B. P. Kersevan, E. Richter-Was, *The Monte Carlo event generator AcerMC versions 2.0 to 3.8 with interfaces to PYTHIA 6.4, HERWIG 6.5 and ARIADNE 4.1*, Comput. Phys. Commun. **184**, 919 (2013)
- [32] B. Abi, et al., *Mis-identified lepton backgrounds to top quark pair production*, ATL-COM-PHYS-2010-849 (2010)
- [33] K. Becker, et al., *Mis-identified lepton backgrounds in top quark pair production studies for EPS 2011 analyses*, ATL-COM-PHYS-2011-768, (2011)
- [34] M. Lehmann, *b-Tagging Algorithms and their Performance at ATLAS*, arXiv:0809.4896v3 [hep-ex] (2008)
- [35] R. Brun, F. Rademakers, *ROOT: An object oriented data analysis framework*, Nucl. Instrum. Meth. **A389**, 81 (1997)
- [36] ATLAS Collaboration (G. Aad, et al.), *b-Jet Tagging Efficiency Calibration using the System8 Method*, ATLAS-CONF-2011-143 (2011)
- [37] O. Behnke, K. Kröninger, G. Schott, T. Schörner-Sadenius, *Data Analysis in High Energy Physics: A Practical Guide to Statistical Methods*, Wiley (2013)

Acknowledgements

First, I would like to thank Prof. Dr. Arnulf Quadt for giving me the opportunity to write my bachelor's thesis in particle physics and also for being the first referee. I am also very thankful to Prof. Dr. Ariane Frey for being the second referee and for awakening my interest in particle physics by giving very inspiring lectures.

I also would like to thank Priv.-Doz. Kevin Kröninger for supervising me and discussing the achieved results and proof-reading my thesis. His ability to make physics understandable is incomparable.

A thousand thanks to Philipp Stolte for being my supervisor and always being available when I needed help. Also for his patience when solving problems or proof-reading this thesis. Thank you so much!

Additional thanks go to Dominik Müller for helping to start into the project and always knowing the answer to the problems appearing while programming.

Erklärung nach §13(8) der Prüfungsordnung für den Bachelor-Studiengang Physik und den Master-Studiengang Physik an der Universität Göttingen:

Hiermit erkläre ich, dass ich diese Abschlussarbeit selbständig verfasst habe, keine anderen als die angegebenen Quellen und Hilfsmittel benutzt habe und alle Stellen, die wörtlich oder sinngemäß aus veröffentlichten Schriften entnommen wurden, als solche kenntlich gemacht habe.

Darüberhinaus erkläre ich, dass diese Abschlussarbeit nicht, auch nicht auszugsweise, im Rahmen einer nichtbestandenen Prüfung an dieser oder einer anderen Hochschule eingereicht wurde.

Göttingen, den 18. Juli 2014

(Jens Oltmanns)